EAEC05YU-EM06

Exhaust gas dispersion effects under controlled environmental conditions

Bernhard Heiden, Peter Johann Sturm, Gerhard Pretterhofer, Tuan Le An
Institute for Internal Combustion Engines and Thermodynamics, Graz University of Technology, Graz,
Mario Ivanišin, *Magna Steyr Fahrzeugtechnik AG & Co KG, Graz, Austria*





Abstract

Urban air quality is determined by exhaust gas dilution processes. Unfortunately this process is difficult to describe concerning particulate matter. As a consequence the aim of the following experiments was to clarify the dominating processes accompanying the dilution process of vehicle particle emissions.

Ambient air measurements were performed under different size-scaled dilution conditions and under different cold start situations. Coagulation experiments were performed in a 9m long pipe also under cold and warm start conditions. Different nanoparticle quantities were measured among them, the PM_{10} mass with a TEOM (tapered element oscillating microbalance) and the number-size distribution with a SMPS (scanning mobility particle sizer). Additionally the extinction with a SICK extinction measurement device and the humidity was measured.

The cold start emissions lead to particle emissions that consist of two types of particles, first mainly liquid particles and second soot particles. The liquid phase particle emissions disappear after a certain time and a pure soot emission remains. The experiments indicate that the previous state of the engine-tailpipe is of importance for liquid emissions but not for soot emissions, that means that a warmed up system produces less liquid phase emissions.

Cold start particle emissions can be regarded as purely mixed with the ambient atmosphere and an immediate coagulation cannot be assumed. This can be inferred out of the decay from an unimodal into a bimodal number size distribution under dilution conditions, where accumulation of the aerosol occurs, and from coagulation experiments.

A new method for determining a mass density function is derived. This allows for interpreting measurements according to a time dependent liquid uptake with respect to spherical particles.

Keywords: *Exhaust gas dispersion, cold start emissions, ambient air measurement, emission dilution*

1. Introduction

Dilution concerning nanoparticles is up to now an not well understood process. The dilution process itself is of complex physical nature. A lot of disciplines can be integrated for the gas phase only like fluid mechanics, thermodynamics or chemistry. When nanoparticles are formed the complexity increases, as it concerns a lot of sciences furthermore. The particle formation and their dynamics is together difficult to understand and to measure. Therefore it is an approach to pick out some small aspects of this problems and discuss them in the background of a broad range of experiments. First some aspects the gas phase effect for HC in a standardized environment for car exhaust emissions measurement are looked at. Then some experiments of different scales in the environment are presented, indicating the instationary nanoparticle processes resulting from real-like dilution. A coagulation experiment is shown that indicates a similar behavior as in other size scales for particles, both for number decrease and diameter size growth. In the end a new method for integrating time dependent size distribution and mass measurement data is presented resulting in a consistent density calculation. The small scale tunnel was taken as an example.

2. Dilution in a constant volume sampling (CVS) tunnel with respect to HC

Obviously, the standard CVS tunnel is inadequate to demonstrate the ultrafine particle characterization as the dilution factor (usually from 3 to 15) rarely reaches a point where the processes of nucleation, condensation or agglomeration are effectively arrested, like they are in the atmosphere (Colling, 2003). Thus this conventional CVS method is sufficient for making mass-based particle measurements, not for particle size distribution.

Nanoparticles are largely generated during the dilution process as the hot exhaust gas mixes with cool ambient air. The primary mechanism for nanoparticle formation during dilution is homogeneous nucleation of sulphuric acid, onto which either volatile organic compounds or their oxidation products condense. All of these components normally remain in the gas phase at exhaust gas temperatures. Nucleation is however a clearly nonlinear process, which can be very sensitive to a number of variables in the dilution process. These variables have been shown to have a significant effect on nanoparticle production, including overall dilution factor, rate of dilution, turbulence intensity, mixing length-scales, dilution air temperature, humidity, and background particle concentration. In addition to the variability introduced by the dilution, particle formation is also significantly affected by the exact nature of the exhaust gas such as temperature, amount and composition of particles and gas-phase particle precursors, which itself is strongly dependent on the fuel and lubricating oil used, as well as engine operating conditions, mechanical condition of engine components, etc.

Through the measurement and simulation established for raising higher understanding about the dilution tunnel, some of the above observations were again emphasized.

Fig. 1 shows a simulation model of a PDP-CVS (Positive Displacement Pump – Constant Volume Sampling) system at a chassisdynamometer of the Graz Technical University (TUG). Of which, the construction of the CVS tunnel was changed to have the dilution process starting from Mixing-T, by this way, a right part of the dilution tunnel (on the right side of the orifice) is not important to be included in the simulation model. In addition, the dilution tunnel has 4,095 [m] in length and 0,316 [m] in diameter.

The model was solved steady state based on a CFD method. FLUENT software was used for this purpose. It is a k-ε turbulence model with segregated, implicit solver.

Fig. 1 presents also the contours of gas velocity magnitude, where the velocity distribution is clearly shown. In the dilution tunnel, after the orifice, the mixture between exhaust gas and ambient air is gradually homogeneous till the tunnel's end, where the particle mass-based sample probe is located. The velocity of mixture in the dilution tunnel is almost lower than 2 [m/s]. This is an ideal condition for particulate forming, but it is also a good condition for gaseous substances and particulate condensation at the end of the tunnel.

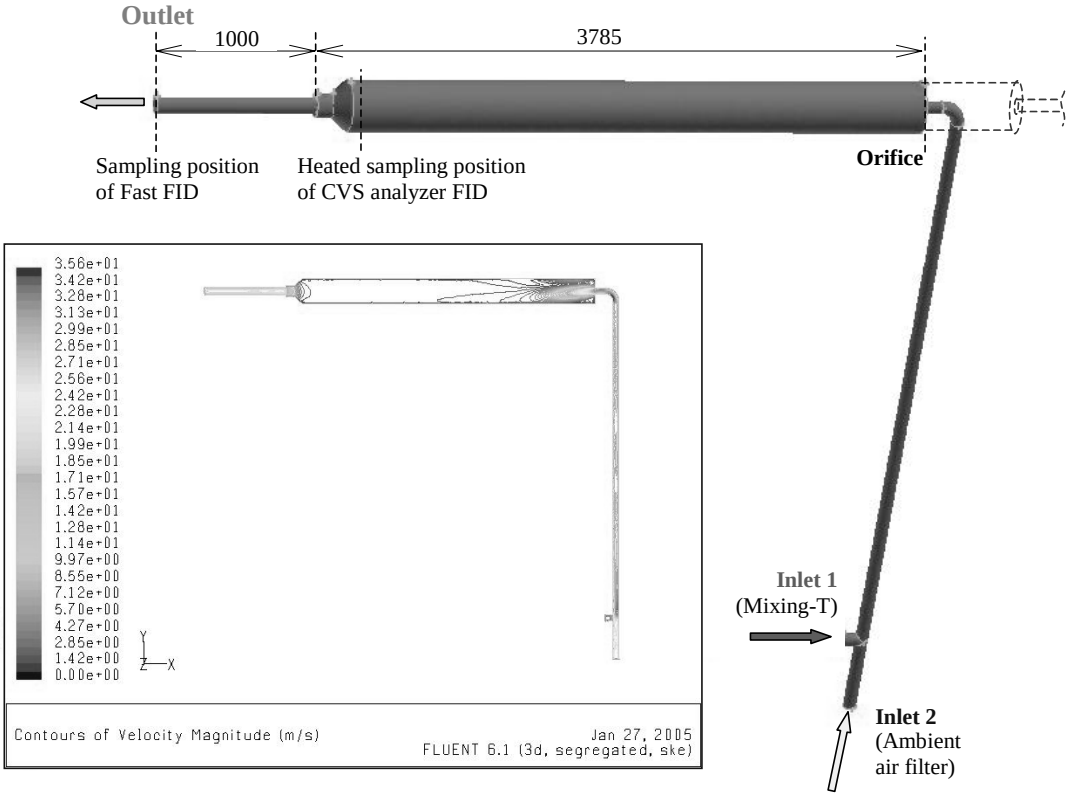

Fig. 1: Model of the dilution pipe and the CVS tunnel

An instantaneous measurement was performed on the chassisdynamometer to investigate the condensation and other effects to hydrocarbon (HC) emission transport through the CVS. Beside the CVS analyzer FID, an extra Fast FID, HFR 500 from Cambustion LTD was used to get the control HC signal. VW Jetta Cat, a Pre-Euro gasoline car was chosen to test on roller test bed following an established driving cycle (Fig. 2 and Le Anh, 2005).

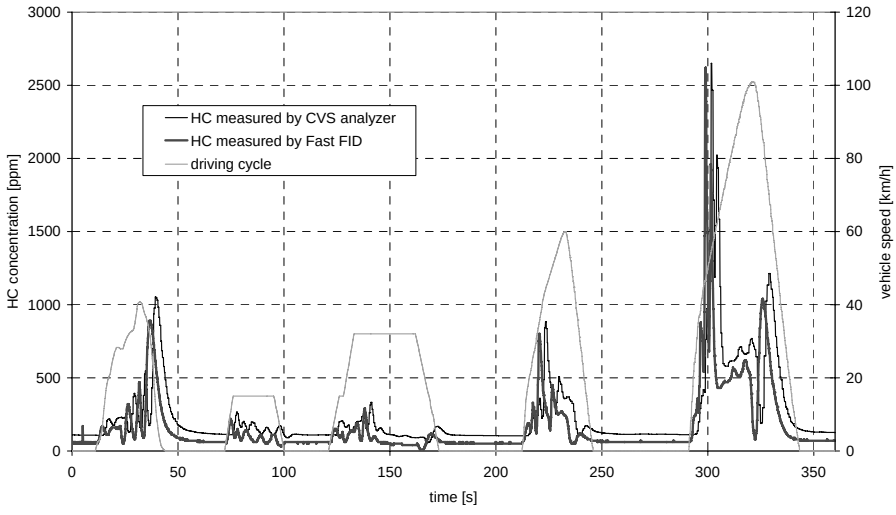

Fig. 2: HC signal measured on roller test bed added by Fast FID

Although the sampling probe of Fast FID was located 1 meter after the dilution tunnel, whereas it was however at heated probe (at the end of the tunnel) of the original CVS (Fig. 2), the HC signal from CVS

analyzer is about 3 seconds delay than that of Fast FID. This can be explained by the length of the sampling line and the analyzer response time.

It is clearly shown that the absolute HC concentration measured by CVS analyzer FID is in general 50 [ppm] higher than that of Fast FID. This difference is due to the condensation of HC at the end of the dilution tunnel as long as the condition for HC reaction is not sufficient. The condensation of HC draws somehow the condensation of particle as the deposition and aggregation of particle happen due to low velocity flow.

3. Outdoor measurements

3.1. Measurement setup

Measurements in two size scales were performed. For the small size scale (campaign #1) a tomatoes-tunnel in the immediate ambient of the exhaust pipe was used (see Fig. 3). This tunnel was 1.5 [m] long and had a half circle geometry with a radius of 0.3 [m].

The second large size scale campaign #2 was performed in a long street tunnel (Gleinalmtunnel) in Styria, Austria during a maintenance operation that is when the tunnel was closed for the whole traffic. Under this condition no car emissions can be detected. The advantage of this situation was that the ventilation could be controlled independent of the traffic. The measurement location in a side tunnel of the Gleinalmtunnel and the measurement setup is depicted in Fig. 3. Two types of experiments were performed in the large scale tunnel: With "ventilation on" (#2.1) and with "ventilation off" (#2.2-3). The state "ventilation on" corresponds to the normal tunnel operation. For the state "ventilation off" a negligible portion of ventilation can be assumed. The exhaust air jalousie was closed but the door to the exhaust shaft was slightly opened. This lead to minimal air velocity from the emission source to the ventilation shaft. By this means backlayering of the exhaust gas could be avoided. For experiment #2.2-3 two types of diesel cars with Pre-Euro engines were used, for experiment #2.2 a passenger car (PC) and for experiment #2.3 a heavy duty vehicle (HDV).

The third measurement campaign #3 was performed nearby the laboratory under ambient dilution conditions. In this campaign the coagulation behavior was investigated first for cold start and second for a warm start emission situation. The same PC was used for all measurement campaigns.

The parameters for all the measurements are depicted in Tab. 1. This also demonstrates the similarity in geometry by the length scaling factor 10 and the velocity and residence time scaling ~5 for experiments #1.1-2 and #2.1. For the coagulation experiments different residence times could be measured. The CVS tunnel is also shown for qualitative comparison.

	small scale		large scale		coagulation	CVS tunnel
parameter	#1.1-2	#1.3	#2.1	#2.2-3	#3.1-2	
velocity u [m/s]	1±0.1	-	~2	~0.02	0.252	~2
volume V [m^3]	0.212	0.212	~375	~375	<<1	0.30
residence time τ [s]	1.5	-	~7	~600	0;12;24;36	~1.9
length L [m]	1.5	1.5	15	15	0;3;6;9	3.8
radius R [m]	0.3	0.3	-	-	0.004	0.158

Tab. 1 Tunnel size scales and parameters

3.1.1. Measurement quantities

Different nanoparticle quantities were measured. For the PM_{10} mass measurement a TEOM (tapered element oscillating microbalance) was used except for campaign #3. The limiting measurement range was set to 10 000 [μg/m^3]. For campaign #1 the measurement location was approximately 15 [cm] above ground and

the same as the SMPS and SICK sampling location. For campaign #2 the measurement distance was approximately 15 [m] away from the exhaust tailpipe.

The nanoparticle number size distribution was measured with a SMPS 3080 (scanning mobility particle sizer) with a DMA 8081 and a CNC 3010 from TSI. The size range was set to 10–400 [nm] and the sample flow was 0.6 [l/min], with a sheath air flow of 6 [l/min] for all campaigns except the coagulation experiments #3.1-2. For experiment #3.1 the sample flow was set to 0.76 [l/min]. As the integrated flowmeter has a strong drift the sample flow was calibrated before the measurements with a bubble flowmeter.

The extinction was measured with a SICK extinction measurement device VICOTEC 414. This instrument was used in campaign #1 with a low length scale of 1 [m] , whereas the normal operation path is 10 [m]. The short length was due to laboratory conditions and can be partly compensated by higher concentrations. The wood construction was only for temporarily measurement purposes and hence extremely sensitive against vibrations. The exhaust gas was flowing through a pipe positioned at the end of the tunnel entering in a 1 [m] long metal pipe with a measurement for the SICK device, then the exhaust sample entered the SMPS. The light sensitivity was overcome by prior calibration. The environmental influence of light was avoided due to operation in the night. For campaign #2 the path length was 10 [m] with an average distance of 15 [m] from the emission source (see Fig. 3).

The humidity and temperatures (Pt 100 sensors) were measured with a DASYLAB data acquisition system (DAQ). The DAQ was used for campaigns #2 and #3. Humidity was only measured in campaign #3. The velocities were measured by an handhold cup anemometer.

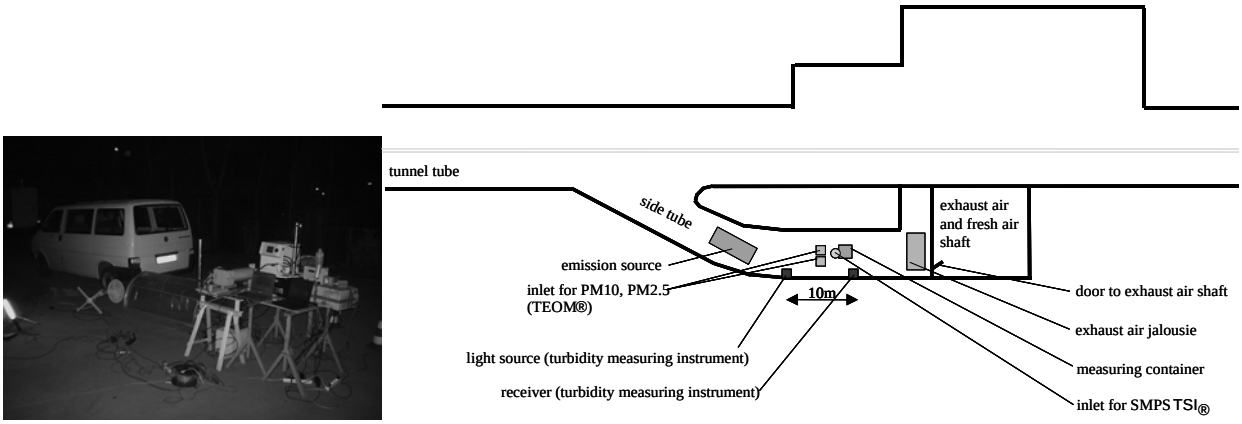

Fig. 3 Measurement campaign #1 on the left side and schematic drawing of campaign #2 in the Gleinalmtunnel on the right side

3.2. Small scale measurement

3.2.1. Experiment #1.1-2

In the small scale measurement a ventilator was used to obtain a constant flow rate through the tunnel. The tunnel was open on both sides that means enough fresh air had diluted the exhaust gas. The flow rate was measured with 1 ±0.1[m/s]. There were first performed two measurements at the same conditions #1.1 and #1.2. The results for the mass and extinction measurements are depicted in Fig. 3. As the TEOM is not responding immediately, although measurement values are per second, the initial concentration is reached after 2 minutes. The same behavior can be observed at the end of the experiment. The first measurement #1.1 has higher emissions and a decreasing mass concentration. The second experiment #1.2 performed 29 minutes after the beginning of the first experiment and after 15 minutes cooling down of the engine has the same tendency ending approximately at the same mass concentrations of 600 [$\mu g/m^3$].

The extinction measurement leads to similar results. The VICOTEC extinction measurement device is first calibrated at ambient air conditions, and has the value 0 that means perfect visibility. As the measurement

begins, after a short delay time a peak can be observed, then the emission reaches a minimum and is rising in the next time. The tendency is the same for both experiments. In the first experiment #1.1 the extinction is higher due to higher particle emissions, in the second experiment #1.2 it is lower due to lower total particle emissions. In both experiments #1.1-2 the tendency is towards a higher extinction although the total mass is decreasing.

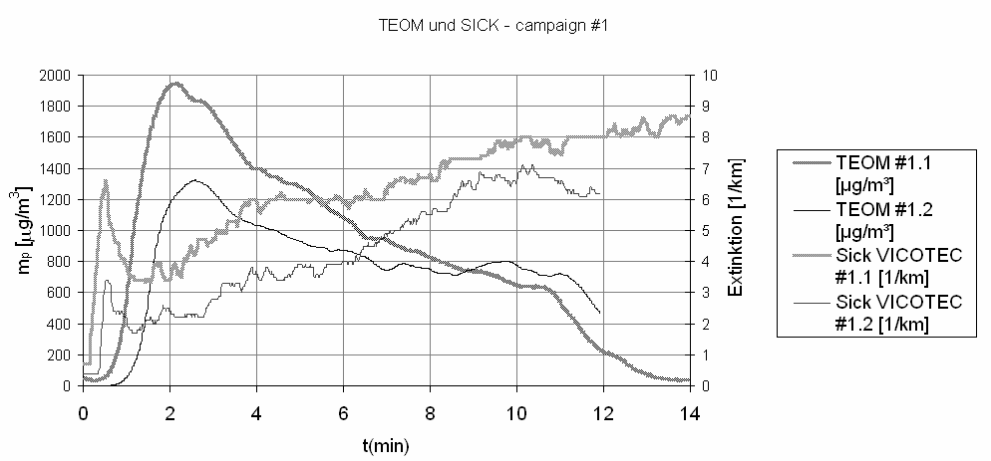

Fig. 4 Two small scale measurements of the ambient particle mass and extinction. Experiment #1.1 and #1.2 are the first and second cold start experiment respectively.

	#1.1				#1.2			
t	4.1	6.1	8.2	10.2	4.1	6.1	8.2	10.2
N_{tot}	4.83E+06	4.89E+06	4.96E+06	4.47E+06	4.56E+06	4.30E+06	4.88E+06	5.53E+06
$\ln(\sigma_g)$	0.425	0.423	0.431	0.474	0.473	0.510	0.491	0.489
σ_g	1.530	1.526	1.539	1.606	1.605	1.665	1.634	1.631
dp_g	58	53	48	44	47	44	44	43
N in %	100%	101%	103%	92%	100%	94%	107%	121%
m_p	1837	1320	949	753	1224	1019	858	723

Tab. 2 Parameters of the lognormal distribution of experiment #1.1-2; time in minutes, dp_g in nm and m_p in µg/m³, N_{tot} in #/cm³

3.2.2. Experiment #1.3

In the experiment #1.3 the tunnel was closed. Due to this fact quite a high particle number concentration could be gained (Tab. 3). This experiment is similar to #2.2-3. Both cases can be regarded as fed batch process in the limiting case of a batch reactor. This simulates the condition in the exhaust pipe with a greater residence time according to the volume and exhaust gas flow.

	#1.3			
t	2.1	6.1	8.2	10.2
N_{tot}	1.31E+07	1.23E+07	1.11E+07	9.60E+06
$\ln(\sigma_g)$	0.526	0.549	0.547	0.543
σ_g	1.692	1.731	1.728	1.721
dp_g	96	94	89	86
N in %	100%	94%	85%	73%

Tab. 3 Parameters of the lognormal distribution of experiment #1.3; time in minutes, dp_g in nm, N_{tot} in #/cm^3

All the measurements of #1 are unimodal and can be fitted well with a lognormal distribution. The results for the calculated lognormal distribution are depicted in Tab. 2 and Tab. 3. For experiments #1.1-2 the mass is also shown. The mass concentration of experiment #1.3 was over the limit of 10 000 [µg/m^3] of the TEOM.

3.3. Large scale measurements in the Gleinalmtunnel

3.3.1. Experiment #2.1

For this experiment the normal ventilation was on but there was no traffic. The approximate quantities are shown in Tab. 1. Very low extinction values were measured. The mass and number concentrations were also rather low, which indicates an error of the PM_{10} measurement. The $PM_{2.5}$ control measurement was also out of operation. The number size distribution is depicted in Fig. 5, together with the PM_{10} measurement. The PM_{10} maximum in the beginning can probably be explained by a resuspension of dust due to ventilation. Two effects can be observed. The first unimodal number size distribution decreases with time. The peak is shifted to lower diameters and a small second peak in the accumulation diameter size range becomes visible. Hence the influence of the cold start might have played an important role and coagulation a minor part. Sturm et al. (2003) showed that also for normal traffic operation (in the Plabutschtunnel) there can be found no coagulation in the ventilation shaft although a daytime variation can be measured.

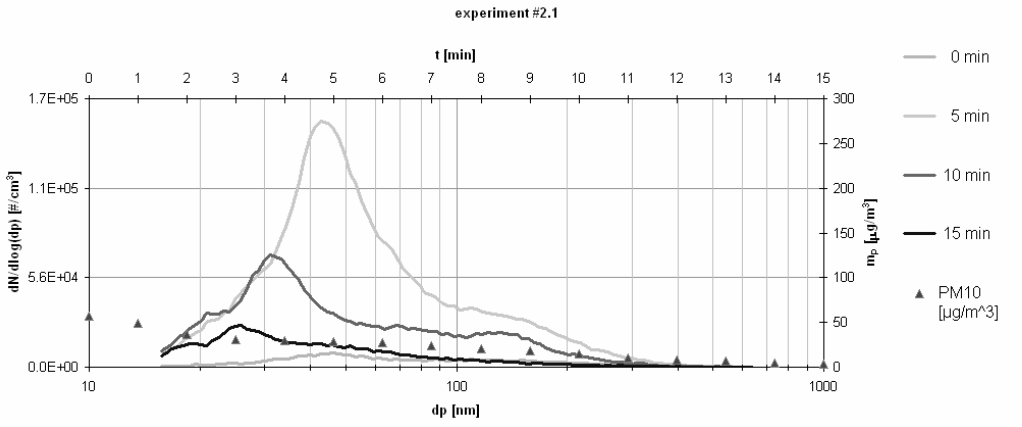

Fig. 5 Particle number size distribution with the PC with a pre-Euro engine and PM_{10} for experiment #2.1

3.3.2. Experiment #2.2-3

For this experiment the ventilation flap was closed and the door was opened for minimal ventilation operation so that the ventilation could be regarded as off. Hence a very low velocity of air could be approximated for ~0.02 [m/s], so that the residence time was ~10 minutes. The particle number size distribution is depicted in Fig. 6. The maximum of the particle number size distribution (as at experiment #2.1) was approximately 45 [nm]. Compared with experiment #2.1 with short residence times and small

mass concentrations there was a large residence time and an accumulation of mass concentration took place. With increasing time the particle numbers with large diameters, within the range of 80 [nm], outweighed particles with small diameters 30 [nm]. Nine minutes after the start a clearly bimodal distribution had evolved. This indicates both evaporating of liquid from particles due to the number decrease and coagulation due to a developing bimodality with a peak in the accumulation diameter size range. Experiment #2.3 showed the same behavior with a more developed accumulation peak and higher mass and number concentrations.

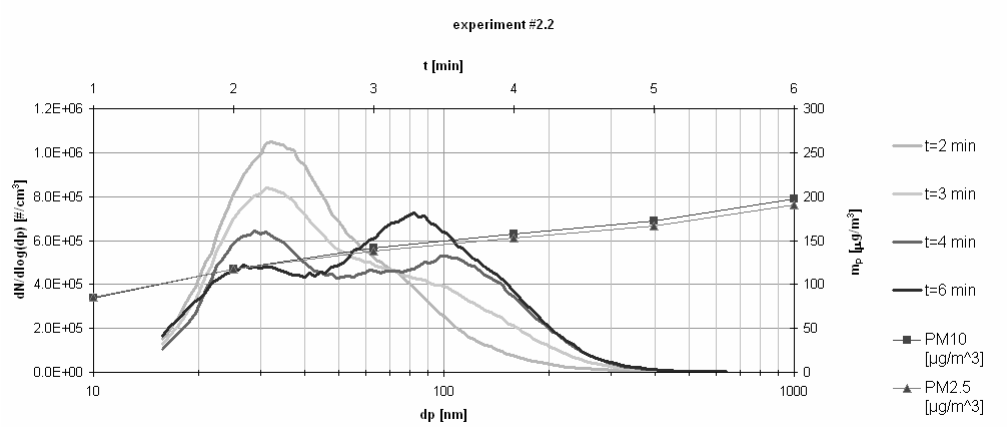

Fig. 6 particle number size distribution for experiment #2.2 with the PC with a pre-Euro engine; the total mass concentration (PM_{10}) is increasing

3.4. Coagulation experiments #3.1-2

The results for the coagulation experiment #3.1 with the cold start situation is shown in Fig. 1 for the number size distribution and the relative humidity. The first bimodal distribution disappears as the engine is getting warm. At the same time the relative humidity ϕ is decreasing from 45% to 28%. The mean temperature was 24±2°C for all measurements. The parameters for the logarithmic normal distribution are given in Tab. 4, although for number size distributions in the beginning this is not a good approximation as there are two overlapping number size distributions.

	#3.1			
t	0	11.9	23.8	35.7
L	0	3	6	9
N_{tot}	1.60E+07	1.41E+07	1.05E+07	8.46E+06
$\ln(\sigma_g)$	0.515	0.485	0.432	0.416
σ_g	1.6733	1.62414	1.54004	1.51648
dp_g	96	94	89	86
N in %	100%	89%	66%	53%
ϕ	45%	48%	38%	28%

Tab. 4 Parameters of the lognormal distribution of the coagulation experiment #3.1; t in minutes, dp_g in nm, N_{tot} in #/cm^3

For the second coagulation experiment #3.2 the humidity stayed at the level of the end of experiment #3.1. In addition a unimodal peak was observed. Hence the nucleation peak consisted probably of a water like substance. The coagulation aimed at lead to the peak in the accumulation mode.

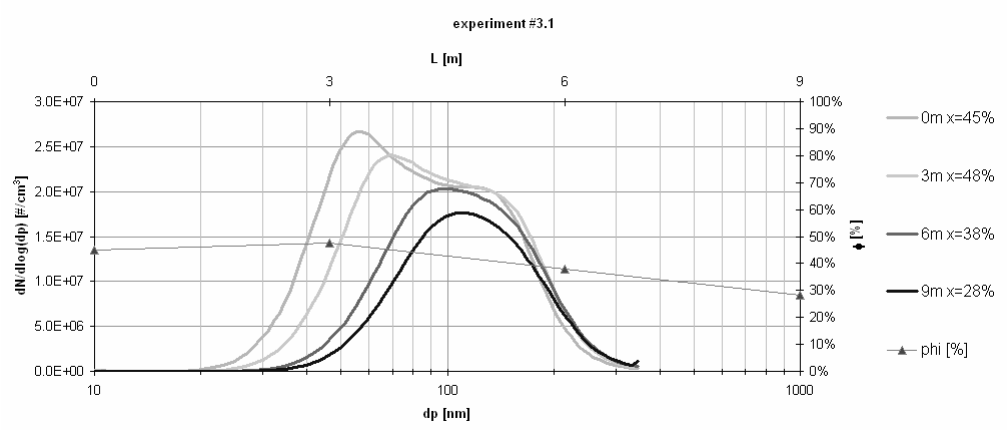

Fig. 7 Coagulation experiment #3.1 number size distributions and the relative humidity ϕ in %

	#3.1			
t	0	11.9	23.8	35.7
L	0	3	6	9
N_{tot}	1.60E+07	1.41E+07	1.05E+07	8.46E+06
$\ln(\sigma_g)$	0.515	0.485	0.432	0.416
σ_g	1.6733	1.62414	1.54004	1.51648
dp_g	96	94	89	86
N in %	100%	89%	66%	53%
ϕ	45%	48%	38%	28%

Tab. 5 Parameters of the lognormal distribution of experiment #3.1; t in minutes from beginning of the cold start, L in m, dp_g in nm, N_{tot} in #/cm^3

4. Density calculations for diluted particles

We can write the concentration c as dependant of different variables (Eq. 1). The measured variables were the mass concentration c and the particle size distribution with time. With the particle size distribution the diameter dp and the total number concentration N can be calculated.

$$c = N \cdot Vp \cdot \rho \qquad \text{Eq. 1}$$

When we write the total differential, introduce the volume relation for a spherical particle and differentiate with t then we get Eq. 2.

$$\frac{\frac{dc}{dt}}{N \cdot Vp} = \left(\frac{dN}{dt} \cdot \frac{1}{N} + \frac{3}{dp} \cdot \frac{ddp}{dt} \right) \cdot \rho + \frac{d\rho}{dt} \qquad \text{Eq. 2}$$

Here we have N, dp, c and their derivatives as values. These can be determined by fitting the experimental data with an exponential fit. The resulting equations are depicted in Eq. 3.

$$N = a_1 \cdot e^{a_2 \cdot t}$$
$$dp = a_3 \cdot e^{a_4 \cdot t} \qquad \text{Eq. 3}$$

$$c = a_5 \cdot e^{a_6 \cdot t}$$

When we apply Eq. 3 in Eq. 2 and simplify the result we get Eq. 4, which is an linear ordinary differential equation of first order.

$$a_7 \cdot e^{a_8 \cdot t} = a_9 \cdot \rho + \frac{d\rho}{dt} \qquad \text{Eq. 4}$$

$$a_7 = \frac{3}{4} \cdot \pi \cdot \frac{a_6}{a_1 \cdot a_3^3}$$

$$a_8 = \left(a_6 - a_2 - 3 \cdot a_4\right)$$

$$a_9 = \left(a_2 + 3a_4\right)$$

The solution of Eq. 4 is given in Eq. 5 with constant ρ_0 that has to be defined from the measurements.

$$\rho(t) = \rho_0 \frac{a_7}{a_8 + a_9} \cdot e^{a_8 \cdot t} \qquad \text{Eq. 5}$$

The experimental results are shown together with the density function from Eq. 5 in Fig. 8. At the end of the experiment a kind of steady state is assumed, as the system itself should produce a steady state. In both cases the (mass) density approaches the compact density of soot at the end of the experiment. The concentration indicates this tendency, as it reaches also the same value at the end. It is interesting that the result of the soot density was only a result of the particle mass and the size distribution measurement. The number distribution and the diameter development behaved different, although the experimental conditions were the same.

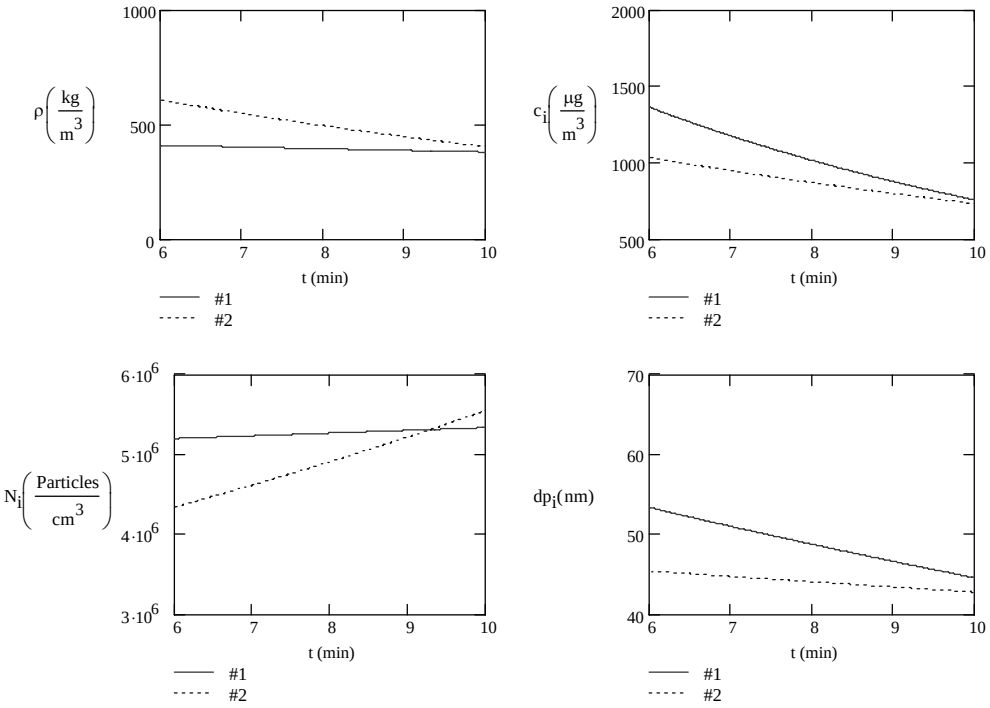

Fig. 8 Density function ρ and experimental results N, c, dp for experiments #1.1 and #1.2

When we have the density function ρ (Eq. 5) and we assume that the pure density at the end is nearly "dry" soot then the density of the mixture is given by Eq. 6, where α is the fraction of water, ρ_w is the density of water and ρ_s is the density of soot.

$$\rho = \alpha \cdot \rho_W + (1 - \alpha) \cdot \rho_S \qquad \text{Eq. 6}$$

The result for the liquid uptake α and for the assumed densities is given in Tab. 6.

ρ_S	ρ_W	$\alpha_{1(t0=6min)}$	$\alpha_{1(tE=10min)}$	$\alpha_{2(t0=6min)}$	$\alpha_{2(tE=10min)}$
kg/m^3	kg/m^3	-	-	-	-
380	1000	4.68%	0.00%	36.65%	3.68%

Tab. 6 mean liquid uptake α of particles; $\alpha = m_W/(m_W+m_S)$

As conclusion of the experiment #1 it can be summarized that under different cold start conditions different ways of liquid uptake of the soot particles are possible, but also a mixture of particles of similar size can be thought. This results in a strongly different pattern of size and number distribution, but it can be regarded plausible when introducing the propose density function ρ. By this way also the percentage of liquid uptake can be calculated.

5. Conclusions

The cold start emissions lead to particle emissions that consist of two types of particles, first mainly liquid particles and second soot particles. The liquid phase particle emissions disappear after a certain time and a pure soot emission remains. The experiments indicate that the previous state of the engine-tailpipe is of importance for liquid emissions but not for soot emissions, that means that a warmed up system produces less liquid phase emissions.

Cold start particle emissions can be regarded as purely mixed with the ambient atmosphere and an immediate coagulation cannot be assumed. This can be inferred out of the decay from an unimodal into a bimodal number size distribution under dilution conditions, where accumulation of the aerosol occurs, and from coagulation experiments.

In addition nanoparticle coagulation experiments show that a high concentration and a considerable residence time is necessary for coagulation. Hence it can be assumed that coagulation can be neglected for CVS measurements but not condensation of hydrocarbons.

A new method for determining a mass density function has been presented. This allows for interpreting measurements according to a time dependent liquid uptake with respect to spherical particles.

6. References

Brown, L. M., Collings, N., Harrison, R. M., Maynard, A., D. and R.L. Maynard (2003). *Ultrafine Particles in the Atmosphere*. The Royal society, London.

Friedlander, S. K. (2000). *Smoke, Dust, and Haze*, Oxford University Press, New York.

Hinds, W. C. (1999). *Aerosol Technology: properties, behavior, and measurement of airborne particles*, John Wiley & Sons, Inc., New York.

Le Anh, T. and S. Hausberger (2005). *Response times in instantaneous emission measurement*, ARTEMIS Task 3156, in print, TUG, Graz.

Sturm, P. J., Baltensperger, U., Bacher, M., Lechner, B., Hausberger, S., Heiden, B., Imhof, D., Weingartner, E., Prevot, A. S. H., Kurtenbach, R., and P. Wiesen (2003). *Roadside measurements of particulate matter size distribution,* Atmospheric Environment, 37, 5273-5281.

7. Nomenclature

Variables	***Units***	***Description***
#		particles
#1,#2,#3, #1.1,#1.2 etc.		experimental campaign for outdoor measurement
a_i		coefficients (i =1..9)
c	$\mu g/m^3$	mass concentration
CFD		computational fluid dynamics
CNC		condensation nucleus counter
CVS		constant volume sampling
dp	nm	particle diameter
FID		flammable ionization detector
HC		hydrocarbon
HDV		heavy duty vehicle
lognormal distribution		a good description can be found in Friedlander (2000) and Hinds (1999)
m	kg	mass of all particles
N	$\#/cm^3$	particle concentration
PC		passenger car
PDP		positive displacement pump (ROOT compressor)
SMPS		Scanning mobility particulate sizer – measurement device for nanoparticle size distributions
t	min	time; usually from the beginning of the experiment
t0	min	time in the beginning
tE	min	time at the end
TEOM		tapered element oscillating microbalance
TUG		Technical University Graz
V	m^3	volume of fluid
Vp	m^3	particle volume
α		liquid uptake; in the example the liquid is water: $m_w/(m_W+m_S)$
ϕ (phi)		relative humidity
ρ	kg/m^3	density (function)
ρp	kg/m^3	particle density
σ		standard deviation
τ	t	residence time

Subscripts	***Description***
g	geometric
i	i...experiment number;
m	mean
p	concerning particles
s	soot
tot	total
w	water